Structural Interactions between Horseradish Peroxidase C and the Substrate Benzhydroxamic Acid Determined by X-ray Crystallography[†,‡]

Anette Henriksen,*[,§] David J. Schuller,[||] Kåre Meno,[§] Karen G. Welinder,[⊥] Andrew T. Smith,[#] and Michael Gajhede[§]

Department of Chemistry, University of Copenhagen, Universitetsparken 5, DK-2100 København Ø, Denmark, Department of Molecular Biology and Biochemistry, University of California, Irvine, California 92697-3900, Department of Protein Chemistry, Institute of Molecular Biology, University of Copenhagen, Øster Farimagsgade 2A, DK-1353 København K, Denmark, and School of Biological Sciences, University of Sussex, Brighton BN1 9QG, United Kingdom

Received January 29, 1998; Revised Manuscript Received March 31, 1998

ABSTRACT: The three-dimensional structure of recombinant horseradish peroxidase in complex with BHA (benzhydroxamic acid) is the first structure of a peroxidase−substrate complex demonstrating the existence of an aromatic binding pocket. The crystal structure of the peroxidase−substrate complex has been determined to 2.0 Å resolution with a crystallographic *R*-factor of 0.176 (*R*-free = 0.192). A well-defined electron density for BHA is observed in the peroxidase active site, with a hydrophobic pocket surrounding the aromatic ring of the substrate. The hydrophobic pocket is provided by residues H42, F68, G69, A140, P141, and F179 and heme C18, C18-methyl, and C20, with the shortest distance (3.7 Å) found between heme C18-methyl and BHA C63. Very little structural rearrangement is seen in the heme crevice in response to substrate binding. F68 moves to form a lid on the hydrophobic pocket, and the distal water molecule moves 0.6 Å toward the heme iron. The bound BHA molecule forms an extensive hydrogen bonding network with H42, R38, P139, and the distal water molecule 2.6 Å above the heme iron. This remarkably good match in hydrogen bond requirements between the catalytic residues of HRPC and BHA makes the extended interaction between BHA and the distal heme crevice of HRPC possible. Indeed, the ability of BHA to bind to peroxidases, which lack a peripheral hydrophobic pocket, suggests that BHA is a general counterpart for the conserved hydrogen bond donors and acceptors of the distal catalytic site. The closest aromatic residue to BHA is F179, which we predict provides an important hydrophobic interaction with more typical peroxidase substrates.

Horseradish peroxidase (HRPC)[1] is an oxidoreductase extensively studied by various types of spectroscopy and other techniques. HRPC catalyzes the H_2O_2-dependent oxidation of a variety of aromatic electron donor molecules (AH) through the formation of intermediate compounds (*1*).

$$[\mathrm{Fe(III)(Porp)}] + H_2O_2 \rightarrow \underset{\text{compound I}}{[\mathrm{Fe(IV){=}O(Porp)^{\bullet+}}]} + H_2O \quad \text{(i)}$$

$$[\mathrm{Fe(IV){=}O(Porp)^{\bullet+}}] + \mathrm{AH} \rightarrow \underset{\text{compound II}}{\mathrm{H^+[Fe(IV){=}O(Porp)]}} + \mathrm{A^{\bullet}} \quad \text{(ii)}$$

$$\mathrm{H^+[Fe(IV){=}O(Porp)]} + \mathrm{AH} \rightarrow [\mathrm{Fe(III)(Porp)}] + \mathrm{A^{\bullet}} + H_2O \quad \text{(iii)}$$

The high oxidation state intermediate compound I comprises an oxyferryl heme (*2*) and a porphyrin cation radical (*3*). Compound I reacts with the reducing substrate by extracting a proton and an electron from it. The electron reduces the porphyrin cation radical, and a proton acceptor, generally believed to be the distal histidine, binds the proton. An additional single electron-transfer step returns the enzyme to the resting state by reaction with another aromatic donor molecule. While the first part of the reaction (i) is structurally well characterized (*4*−*6*), the precise mode of interaction between peroxidase and reducing substrates remains more obscure. For HRPC, a range of substrate molecules have been shown to form stable 1:1 complexes in the absence of

[†] This work was supported by the Danish National Research Foundation, the Danish Natural Science Research Council (No. 11-9136), the U.S. National Science Foundation (No. MCB-9405218), and the EU Human Capital and Mobility program (No. ERB CHRX-CT92-0012-130). The European Union supported the work at HASYLAB, EMBL Hamburg outstation through the HCMP Access to Large Installations Project (No. CHGE-CT93-0040).

[‡] The atomic coordinates and structure factors for the HRPC−BHA complex (codes 2atj and r2atjsf) have been deposited in the Protein Data Bank, BNL, Upton, NY.

* Address correspondence to this author of the Department of Chemistry, University of Copenhagen, Universitetsparken 5, DK-2100 København Ø, Denmark. Telephone: +45 35 32 02 73. Fax: +45 35 32 02 99. E-mail: anette@jerne.ki.ku.dk.

[§] Department of Chemistry, University of Copenhagen.

[||] University of California.

[⊥] Institute of Molecular Biology, University of Copenhagen.

[#] University of Sussex.

[1] Abbreviations: ARP, *Arthromyces ramosus* peroxidase; BHA, benzhydroxamic acid; CCP, yeast cytochrome *c* peroxidase; HRPC, horseradish peroxidase C.

S0006-2960(98)00234-7 CCC: $15.00
Published on Web 05/14/1998

hydrogen peroxide (*7* and references cited therein; *8*−*10*). On the other hand, peroxidases are known to be nonspecific in their substrate requirements. Recently, a general correlation has been observed between the rate of reaction of compound I and the half-potential for the formation of the respective radical product (*11*). Also, the energy levels of the lowest occupied molecular orbital of the substrate correlate well with the reaction rate of compound I with substrates (*12*).

Structural determinants of plant peroxidase substrate specificity have been examined through reactions with alkyl- and phenylhydrazines (*13*−*15*). The reaction of phenylhydrazine with the heme group is limited to the so-called exposed heme edge, which includes the heme C20 and heme C18-methyl group. In horseradish peroxidase, this is taken as evidence of a restricted accessibility to the heme ferryl oxygen mediated by the protein environment. The restricted accessibility suppresses oxygen transfer reactions, forcing electron transfer to occur at the heme C20 edge. In support of this, NMR spectroscopy has shown aromatic donor molecules to bind close to the heme C18-methyl (*7*, *16*, *17*). Two-dimensional NMR spectroscopy has revealed two Phe residues in the heme vicinity, one of which interacts directly with both BHA and physiologically relevant substrates such as ferulic acid (*18*) and indole-3-propionic acid (*19*). This particular Phe residue was also shown to interact with the heme C18-methyl and with another nearby Phe residue. Recent modeling (*20*) and NMR studies of mutant HRPC (*21*) have attempted to identify the residue concerned, with the principal candidates suggested from these two studies being F179, F68, and F221. A recent crystal structure of the HRPC resting state (*22*) strongly suggested F179 as the key residue. This has recently been confirmed by NMR analysis of the appropriate HRPC mutant (*23*).

The substrate molecule, BHA, examined in this and in previous NMR studies, is a weak acid ($pK_a = 8.8$) with no established physiological role. Structurally it is related to aromatic peracids, which are potent oxidants of resting state HRPC (*24*). BHA reacts with compound II with a second-order rate constant of 7.8×10^5 M^{-1} s^{-1} (*25*), and it is a competing substrate during the oxidation of phenols and aromatic amines (*26*). The structure of the HRPC−BHA complex may provide information on the interaction of aromatic peracids with the enzyme during compound I formation and the interaction of reducing substrates during compound I and compound II reduction. BHA is not hydrolyzed by HRPC in the absence of peroxide, but it forms a stable, reversible complex with a dissociation constant of 2.4 μM. The ternary HRPC−BHA−CN complex has a considerably higher dissociation constant of 0.15 mM (*26*). Resonance Raman studies of the HRPC−BHA complex have shown that this complex differs from that formed between HRPC and other aromatic donors. The predominantly five-coordinate high-spin heme iron in native HRPC is in the HRPC−BHA complex reported to be perturbed to a six-coordinate high-spin state with a water molecule bound as the sixth ligand (*27*, *28*). A recent NMR study, however, concludes that this complex is five-coordinate (*29*).

A number of NMR studies of substrate complexes have focused on the low-spin HRPC−BHA−CN complex (*7* and references therein; *18*, *30*, *31*), although it is recognized that this complex is distinct compared to that formed between BHA and the native enzyme (*7*). La Mar et al. (*30*) found the ternary HRPC−BHA−CN complex to be heterogeneous, with two forms in rapid exchange. This was attributed to an alternate conformation of a distal residue that sterically blocks the substrate binding site in one of the binding modes. NOE interactions exist between BHA and the heme C18-methyl and between BHA and His42 in the HRPC−BHA−CN complex, suggesting a distal binding site in close proximity to the heme C18-methyl (*21*, *32*). A number of other resonance signal perturbations from, e.g., R38 are consistent with perturbation of the distal heme-linked hydrogen-bonding network.

EXPERIMENTAL PROCEDURES

Crystallization. Crystals were grown by cocrystallization of recombinant HRPC (*33*) and BHA by equilibration of hanging drops against reservoirs of 1.0 M $(NH_4)H_2PO_4$ and 0.1 M cacodylate buffer at pH 6.5 at 283 K. The starting concentration of BHA in the drops was 0.35 mM and the HRPC concentration 6.0 mg/mL, giving greater than 99% complex. The crystals were monoclinic, space group $P2_1$, with unit cell dimensions $a = 74.9$ Å, $b = 62.3$ Å, $c = 78.0$ Å, and $\beta = 104.4°$. Two molecules per asymmetric unit were estimated from solvent content calculations (*34*). The self-rotation function showed a peak at $(\varphi, \psi, \chi) = (90, 90, 180)$ corresponding to a noncrystallographic 2-fold axis.

Data Collection and Reduction. Diffraction data for HRPC−BHA and HRPC−BHA−$Hg(CH_3COO)_2$ were collected at room temperature on a Rigaku R-axis IIC image plate system with a Rigaku RU200 rotating anode operated at 50 kV and 180 mA. The crystal to detector distance was 100 mm, the oscillation range was 2.0°, and a typically used exposure time was 30 min. As for HRPC−BHA−K_2PtCl_6, data were collected at HASYLAB, EMBL Hamburg outstation, on beamline X31. Autoindexing and integration of intensities was achieved with Denzo (*35*); the data were averaged and scaled with Scalepack (*35*), while further data processing was done with the CCP4 programs (*36*). Statistics for the X-ray data are given in Table 1. Diffraction data were collected to minimum Bragg spacing ranging from 2 to 2.1 Å. Generally the data suffered from a high degree of mosaicity, typically in the 1.0−1.2° range.

Structure Solution and Refinement. Molecular replacement with the program AMoRe (*37*) used a complete model of peanut peroxidase (*38*) including all protein atoms, heme group atoms, and cations. Data from 20 to 5 Å resolution were used. Rigid-body refinement at 20−3.5 Å resolution of the correct two-molecule solution gave a correlation coefficient of 0.446 and an *R*-factor of 0.452. Phases generated from the molecular replacement solution were used to solve heavy-atom derivatives by difference Fourier. A $Hg(CH_3COO)_2$ and a K_2PtCl_6 derivative proved useful with 2 and 12 derivative sites, respectively. Statistics for the MIR phases are summarized in Table 1. The molecular replacement solution was truncated to a poly-Ala model and used to calculate model phases to 3.5 Å, which were then combined with MIR phases with the program SIGMAA (*39*). The combined phases were extended to 2.3 Å resolution using solvent leveling, histogram matching, 2-fold noncrystallographic symmetry averaging, and partial structural information using MAGICSQUASH (*40*). The resulting phases were used to begin model fitting with the graphics

Table 1: Statistics for Crystallographic Structure Determination

	HRPC−BHA	BHA−HRPC−$Hg(CH_3COO)_2$	BHA−HRPC−K_2PtCl_6
data collection statistics			
collection site	Home source, image plate	Home source, image plate	EMBL Hamburg, image plate
wavelength (Å)	1.54	1.54	0.996
resolution range (Å)	28.6−2.0	30.0−2.5	20.0−2.3
observations	144839	83705	180404
unique reflections	46595	24189	31247
completeness (%)	98.5	99.5	76.4
R_{merge} (%)[a]	8.5	9.8	7.3
outer resolution shell			
resolution range (Å)	2.00−2.10	2.50−2.63	2.26−2.31
unique reflections	6337	3423	523
completeness (%)	92.8	97.9	25.8
I/sigma(*I*)	3.3		
R_{merge} (%)[a]	20.9		
heavy-atom phasing			
R_{iso} (%)[b]		10.6	12.1
R_{cullis},[c] acentric		0.89	0.84
phasing power,[d] acentric		0.83	1.05
phasing power,[d] centric		0.63	0.84
refinement statistics			
resolution range (Å)	28.6−2.0		
unique reflections	46515		
R-factor[e]	0.176		
protein atoms	2386		
cations	2		
heme atoms	43		
BHA atoms	10		
water molecules	181		
rmsd bond length (Å)	0.006		
rmsd bond angles (deg)	1.09		
mean *B*-factor (Å^2)			
protein	13.5		
water	27.2		

[a] $R_{merge} = \sum_h\sum_i|I_i(h) - \langle I(h)\rangle|/\sum_h\sum_i I_i(h)$. [b] $R_{iso} = \sum_h|F_{PH} - F_P|/\sum_h F_P$. [c] $R_{cullis} = \sum_h||F_{PH} \pm F_P| - F_{H(calc)}|/\sum_h|F_{PH} - F_P|$. [d] Phasing power $= \sum_h F_{H(calc)}/\sum_h||F_{PH} \pm F_P| - F_{H(calc)}|$. [e] $R_{factor} = \sum_h|F_{(obs)} - F_{(calc)}|/\sum_h F_{(obs)}$.

program O (*41*). Phase refinement and extension with 8-fold noncrystallographic symmetry averaging across the two crystal forms of HRPC (*22*) was performed with MAGIC-SQUASH interspersed with model building and refinement. All refinement was carried out using X-PLOR (*42*) with Engh and Huber parameters (*43*), standard protocols for conjugate gradient minimization, simulated annealing, strict noncrystallographic symmetry between the two molecules in the asymmetric unit, and bulk solvent correction. The final part of the refinement was carried out using X-PLOR version 3.851. The quality of the model is shown in Table 1. The *R*-factor of the model is 0.176 including all data from 28 to 2.0 Å resolution with a bulk solvent correction but no σ cutoff applied. The free *R*-factor based on 10% of all reflections was 0.197. A test data set was selected in shells by DATAMAN (*44*) to avoid reflections in the working data related by the noncrystallographic symmetry to test data. The Ramachandran plot shows no residues in disallowed regions and only one residue, T288, in the generously allowed regions. Water molecules were included in the model based on the $F_o - F_c$ electron density by the automated X-PLOR procedure, with a significance level of 3σ. Only peaks returning a well-shaped $2F_o - F_c$ density were retained. The shape of a coherent $F_o - F_c$ electron density in the distal heme crevice guided the inclusion of the substrate molecule BHA in the model (Figure 3). The position of the solvent molecule above the heme iron was refined in alternative ways: including/excluding the van der Waals terms for this molecule in the simulated annealing minimization. The results were slightly different. Including the van der Waals terms gave a distance between heme iron and solvent molecule of 2.8 Å, while exclusion of the terms gave a distance of 2.6 Å. It could be argued that van der Waals interactions should be taken into account, considering the resolution of the data and the distance 2.6−2.8 Å between heme iron and the solvent molecule. However, the van der Waals terms were omitted for the final structural model to avoid a potential bias caused by the electrostatic field that could override a possible weak covalent interaction between the iron and the water molecule.

RESULTS AND DISCUSSION

Structure. Recombinant HRPC is a monomeric enzyme with a molecular mass of 34 kDa, consisting of 309 residues including an N-terminal Met, a heme, and 2 structural calcium ions (*33*). As distinct from the wild-type enzyme that contains eight heterogeneous N-linked glycans (*45*), recombinant HRPC is nonglycosylated. Thirteen α-helices dominate the structure: 14−28 (A), 32−44 (B), 77−90 (C), 97−111 (D), 131−137 (D′), 145−153 (E), 160−171 (F), 181−185 (F′), 199−208 (F″), 232−238 (G), 245−252 (H), 260−267 (I) and 270−284 (J). Two short antiparallel β-strands, 174−176 (β1) and 218−220 (β2), flank the large plant peroxidase insert between helices F and G. The overall fold of the molecule is identical to the previously published structure of native HRPC (*22*). An N-terminal Met (Met0) originating from the translation initiation codon required for *E. coli* expression is included in the present structure. The rmsd between native HRPC crystallized in space group $P3_112$ and the HRPC−BHA complex crystallized in $P2_1$ is 0.3 Å for equivalent backbone atoms and 1.0 Å for side chains, and no part of the structures have an rmsd for backbone

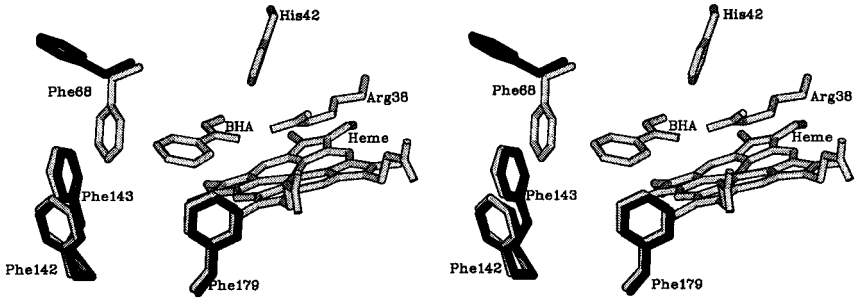

FIGURE 1: Stereoview of the BHA binding site of HRPC. The structure of the HRPC−BHA complex is in gray. The superimposed Phe residues of native HRPC (*22*) are in black. The amino acid residues depicted are the Phe residues in the BHA proximity. His42 and Arg38 are included to help orient the viewer.

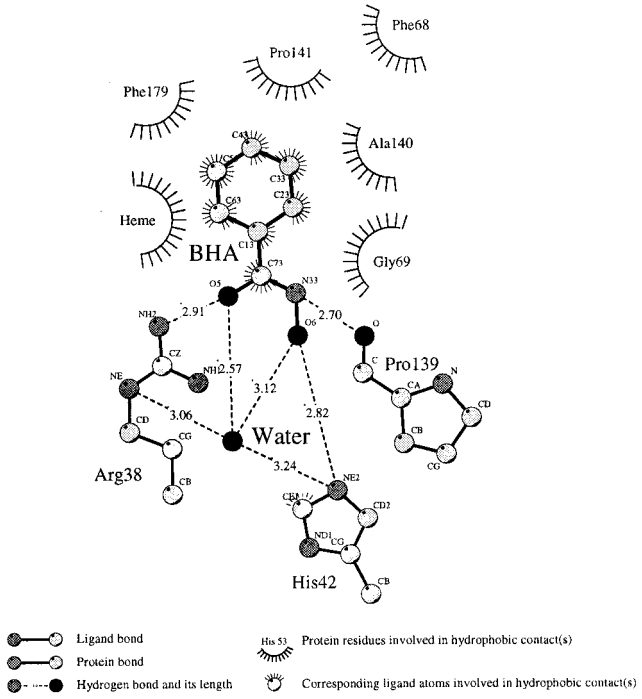

FIGURE 2: LIGPLOT (*57*) diagram of the interactions between BHA and HRPC. Hydrogen bonds and hydrophobic contacts were calculated with HBPLUS (*58*) using the default criterions. Hydrophobic contacts are interpreted by following the spokes protruding from a ligand atom toward a protein residue, shown in the diagram as an arc. Spokes radiating back toward the atom indicate a potential interaction.

atoms larger than 1.0 Å. After solution of the structure, we found the F68 reoriented compared to native HRPC. As a consequence of the reorientation of F68, the face of the aromatic ring of this residue is almost perpendicular to the face of the aromatic ring of BHA. However, the interaction between these aromatic rings is between edges and is not a favorable electrostatic interaction between the oppositely charged edge and center of the two aromatic rings. Additionally, F68 makes a hydrophobic stacking with a proline residue from a symmetry-related molecule. In this interaction, there is no offset in the position of the aromatic rings; the rings stack one above the other.

Interactions between BHA and HRPC. The aromatic donor binding region of HRPC with BHA bound is shown in Figure 1, with a schematic representation of the patterns of interaction between BHA and HRPC given in Figure 2. A list of nonbonded contacts < 4 Å between the molecules is given in Table 2. The electron density of BHA is well-defined, as is the electron density of a solvent molecule

Table 2: Nonbonded Interactions between BHA and HRPC

BHA atom	HRPC atom	distance (Å)
C13	Gly69C_α	3.8
C23	Gly69C_α	3.9
C23	Ala140C_α	3.9
C33	Phe68$C_{\delta 2}$	3.9
C33	Phe68$C_{\epsilon 2}$	3.6
C33	Gly69C_α	3.8
C33	Pro141C_δ	3.8
C43	Phe68$C_{\epsilon 2}$	3.8
C43	Phe68C_ζ	3.7
C43	Gly69C_α	3.8
C43	Pro141C_δ	3.8
C53	Gly69C_α	3.8
C53	Phe179$C_{\epsilon 1}$	3.6
C53	Phe179C_ζ	3.6
C53	heme C18-methyl	3.9
C63	Gly69C_α	3.7
C63	heme C18	3.9
C63	heme C18-methyl	3.7
C73	His42$C_{\epsilon 1}$	3.8
C73	heme C20	3.7

within hydrogen bonding distance of BHA O5. This water is readily distinguishable from BHA (Figure 3). We interpret the minor connectivity in the $F_o - F_c$ map between the solvent molecule and BHA as being due to a high mosaicity in the data. It is, however, also possible that it reflects a small fractional occupation of an alternate binding mode with the BHA molecule being rotated 180° about the aromatic plane.

The hydrophilic portion of BHA makes hydrogen bonds to the distal catalytic His, BHA O6−H42N$_{\epsilon 2}$ (2.8 Å), to the distal Arg, BHA O5−R38N$_{\eta 2}$ (2.9 Å), to a backbone oxygen, BHA N33−P139 O (2.7 Å), and to a solvent molecule above the heme iron, BHA O5−water (2.6 Å) and BHA O6−water (3.1 Å). The distance between the heme iron and the solvent molecule is 2.6 Å (Figure 4). This is significantly shorter than the distance between the heme iron and a corresponding solvent molecule in the structure of native HRPC (3.2 Å) (*22*). However, 2.6 Å is still considerably longer than the 2.1 Å heme Fe−F bond distance in the six-coordinate high-spin cytochrome *c* peroxidase (CCP)−fluoride complex (*46*), and longer than what is generally considered to be a ligand bond distance for iron. Accepting that 2.6 Å is close enough to influence the electronic structure of the heme system, this is in agreement with solution-based resonance Raman studies assigning the HRPC−BHA complex as six-coordinate high-spin with hydrogen bonds from the sixth ligand to either distal His or Arg (*27*, *28*).

The hydrophobic contacts between BHA and F68, G69, A140, P141, F179, and heme C18, heme 18-methyl, and

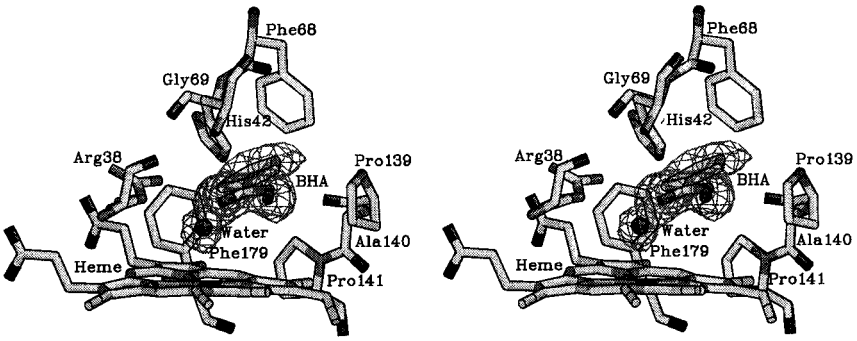

FIGURE 3: Simulated anneal omit $F_o - F_c$ electron density map contoured at 4σ. The map was calculated by omitting benzhydroxamic acid and water from the phasing model after refinement. The atoms are shaded according to type, and the water molecule is represented by a small sphere.

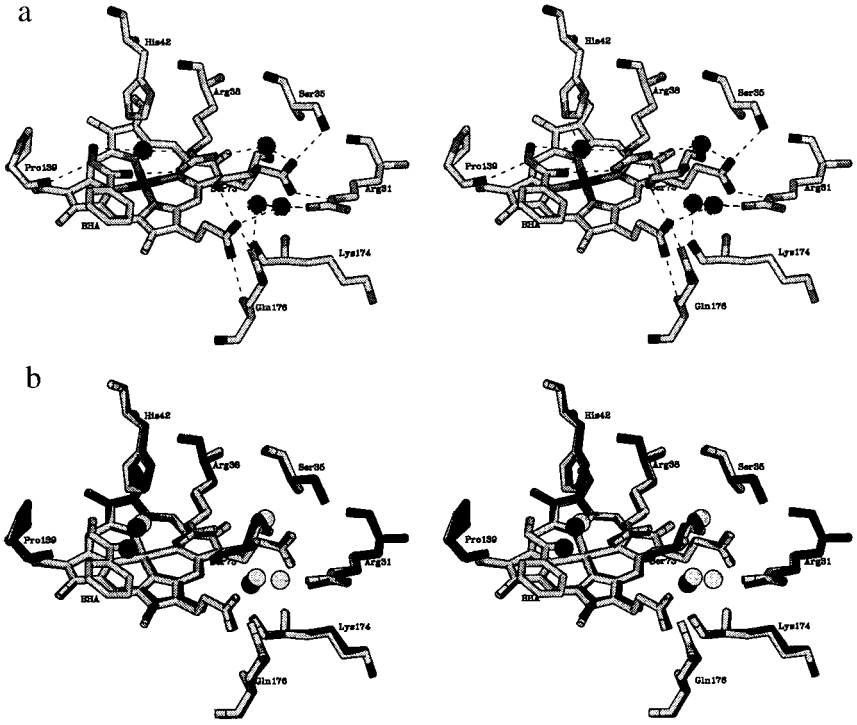

FIGURE 4: (a) The active site of the HRPC−BHA complex with the hydrogen bonds represented by dotted lines and (b) a superimposition of the active site of the HRPC−BHA complex (gray) with the active site of native HRPC (black).

heme C20 (Table 2) can explain the increase in the K_D of the HRPC F68A−BHA mutant complex from 2.4 μM in the wild type to 11 μM in the mutant (*47*). Recent work has shown that the hydrophobic contact with F179 has a more significant effect, since the K_D for the HRPC F179A−BHA complex is 74 μM (*23*). The crystal structure of the HRPC−BHA complex does not reveal higher flexibility of F68 compared to F179, as judge by the temperature factors of the two residues, which are of equal magnitude. However, this might be a consequence of the crystal packing. Comparison of the native HRPC structure and the structure of the HRPC−BHA complex demonstrates that F68 can rearrange unhindered (Figure 1).

BHA as a Model for Oxidizing Substrates. Although aromatic peracids in some ways resemble BHA, they cannot serve as hydrogen bond donors to P139 O. The hydrogen bond donor N33 of BHA is in peracids replaced by an oxygen atom that can only serve as a hydrogen bond acceptor. The distance between N33 and Pro139 O is too short to allow such a replacement to be accommodated without an accompanying structural rearrangement. Therefore, peracids can be expected to bind to HRPC in an alternative orientation, in which there is a 180° rotation around the aromatic plane to bring the α-oxygen in close proximity of the distal His. It is interesting to note that Pro139 is completely conserved in the plant peroxidase superfamily, and the position of its backbone oxygen in the distal heme crevice is invariant in the plant peroxidase crystal structures known. In the structures of native CCP (*48*), native *Arthromyces ramosus* peroxidase (ARP) (*49*), ARP−CN (*50*), and native lignin peroxidase (*51*), a water molecule is within hydrogen bonding distance of Pro139 O. This water is part of a hydrogen bonded network of water molecules leading to the solvent exterior, which in part maps the substrate access channel. When BHA is bound to HRPC, the water above the heme iron is trapped in the protein interior. For an oxidizing substrate to be effective, water must be allowed to leave its position above the heme iron. Since O−O bond cleavage cannot occur in BHA, this molecule is probably not a good model for aromatic peracid substrates, nor is it a guide to the structure of a transient intermediate in compound I formation. However, since BHA

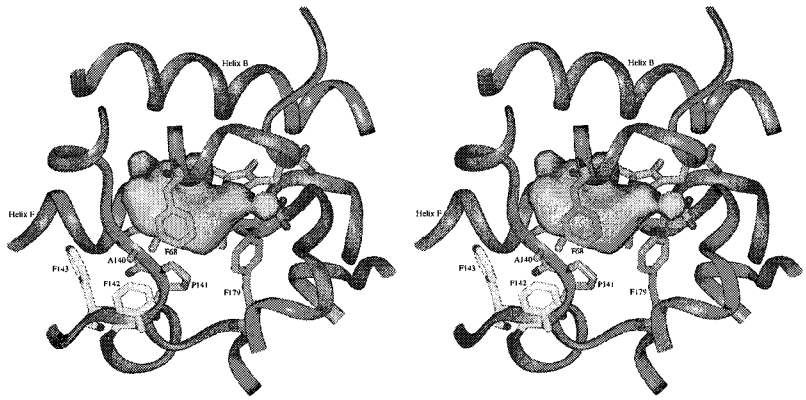

FIGURE 5: Substrate cavity of HRPC−BHA formed by the protein's van der Waals radii. The cavity leads toward the protein exterior with a narrow channel to the right-hand side of F68 and a wider channel to the left of F68. None of the channels are solvent-accessible. A trace of the protein with side chain residues in hydrophobic contact with BHA (dark gray) and F142−F143 (light gray) is included.

also binds to *Coprinus cinereus* peroxidase (alias ARP)(K_D 3.7 mM) (*52*, *53*) which lacks the protein architecture to provide the peripheral hydrophobic contacts shown in Figure 2, BHA must be an excellent structural counterpart for the conserved heme-linked hydrogen bonding network involving H42, R38, and P139. The residues corresponding to H42, R38, and P139 in HRPC are also involved in BHA binding in the ARP−BHA complex (*53*).

BHA as a Reducing Substrate. A rearrangement is seen in the active site of the HRPC−BHA complex, when compared to the structure of native HRPC. The side chain of F68 is reoriented with χ_1 rotated 143° and χ_2 rotated 103°. The reorientation brings F68 into hydrophobic contact with BHA and hinders the access of solvent molecules to the active site (Figure 5). This is in accordance with the finding that 90% of photodissociated CO molecules are trapped in the distal pocket when BHA is bound to HRPC (*54*). It is interesting to note that the corresponding residue in lignin peroxidase, H82, adopts this closed orientation (*51*, *55*). A minor reorientation of 0.7 Å is found for F143, while the rest of the heme crevice and substrate access channel residues show negligible changes in position. One channel on either side of F68 connects the distal heme crevice with the protein exterior. Amino acid residues F68, N70−S73, Q176, R178, and F179 are flanking the channel region on one side of F68, while amino acid residues F68, N135−A140, and F142−F143 are flanking the channel region at the opposite side of F68 (Figure 5). The width of the first channel is 1.8 Å, while the width of the second channel is 2.8 Å. Hence, solvent accessibility to the distal heme crevice is linked to the flexibility of the F68 side chain. It has been demonstrated that the complex between the reducing substrate 2-naphthohydroxamic acid and HRPC has a K_D of 0.2 μM. This is 10 times lower than the K_D of the HRPC−BHA complex (*26*). If we assume the same hydrogen bonds are formed between the 2-naphthohydroxamic acid and HRPC active side residues as in the HRPC−BHA complex, this substrate cannot fit into the aromatic binding pocket, as it is defined in the HRPC−BHA crystal structure (Figure 5). However, a rotation of F68 will allow the 2-naphthohydroxamic acid to extend into the outer region of the channel region toward F142 and F143 (Figure 5).

The crystal structure of HRPC−BHA, the crystal structure of native HRPC, the strong binding of 2-naphthohydroxamic acid, and the wide range of reported reducing substrates for HRPC lead us to conclude that although a well-defined aromatic binding pocket is found in the HRPC−BHA complex, the outer part of the binding pocket is flexible and will accommodate a wide range of substrates more bulky than BHA. Indeed, this is consistent with considerable NMR evidence for such a model [(*21*) and references cited therein].

Superposition of HRPC−BHA and ARP−CN (*50*) complexes suggests that the shortest distance between BHA and a ferryl oxygen will be 3.0 Å. However, if the CN complex resembles the structure of a putative transient intermediate, then the 1.3 Å movement of the distal Arg toward the ferryl oxygen observed in CCP compound I must be taken into account (*4*), as this movement will diminish the substrate accessibility to the oxyferryl center and dictate a change in the binding mode for BHA to compound I.

Implications for the Interactions between BHA and the HRPC−CN Complex. Many NMR studies of interactions between reducing substrate and peroxidases have been conducted on the HRPC−CN complex. The HRPC−CN complex is thought to resemble a putative intermediate preceding the formation of compound I, since HCN binds to HRPC with co-protonation of the distal His and the bound anion being a diatomic molecule. The actual position of the cyanide in the X-ray structure of the ARP−CN complex (*50*) and the 200-fold higher K_D of BHA for the ternary HRPC−BHA−CN complex compared with that of the binary HRPC−BHA complex (*26*) suggest a competition between BHA and cyanide for H-bonding interactions in the HRPC−BHA−CN ternary complex. Superimposition of the structures of ARP−CN and HRPC−BHA gives an interatomic distance of 2.2 Å between cyanide N and BHA carbonyl O5. However, this separation is too short for hydrogen bonding interactions. Furthermore, the hydrogen bond between H42N$_{\epsilon 2}$ and BHA hydroxyl O6 must be absent in the ternary complex, as the distal His is protonated in the complex (*56*). To compensate for the changes in the active site of the CN complex, BHA must bind in a different orientation in the ternary complex. It may be translated toward the periphery of the substrate access channel and possibly adjusted to bring BHA O6 within hydrogen bonding distance of P139 O. This reorientation extends the aromatic portion of BHA to the outer channel region (Figure 5) and decreases the distance between the aromatic portion of BHA and the heme 17-propionate, an interaction observed in NMR studies of the HRPC−BHA−CN complex (*31*). This reorientation would not necessarily require a reorientation of F68, and the distal heme crevice would still be inaccessible

to solvent. The flexibility of F68 observable on the NMR time scale could allow BHA to be bound to HRPC in two alternative modes: an open solvent accessible and a closed solvent inaccessible orientation. These suggestions can explain the two binding modes observed by NMR for the ternary CN complex (*30*), and the change in the equilibrium between the two binding modes observed in the site-directed mutants F68A and F142A (*21*, *47*).

Conclusions. The crystal structure of the HRPC−BHA complex shows that BHA is an atypical reducing substrate with a unique hydrogen bonding potential for the active site residues of the distal heme pocket. Most other reducing substrates do not possess the potential to make these unique interactions and will therefore depend more on the hydrophobic interactions which characterize the peripheral region of the substrate channel of HRPC in particular (*22*). This peripheral hydrophobic patch presumably functions as a binding site or trap for reducing aromatic substrates near heme C18-methyl, without allowing direct access to the ferryl oxygen.

REFERENCES

1. Dunford, H. B. (1991) in *Peroxidases in chemistry and biology* (Everse, J., and Grisham, M. B., Eds.) pp 1−24, CRC Press, Boca Raton.
2. Moss, T. H., Ehrenberg, A., and Bearden, A. J. (1969) *Biochemistry 8*, 4159−4162.
3. Dolphin, D., Forman, A., Borg, D. C., Fajer, J., and Felton, R. H. (1971) *Proc. Natl. Acad. Sci. U.S.A. 68*, 614−618.
4. Fülöp, V., Phizackerley, R. P., Soltis, S. M., Clifton, I. J., Wakatsuki, S., Erman, J., Hajdu, J., and Edwards, S. L. (1994) *Structure 2*, 201−208.
5. Miller, M. A., Shaw, A., and Kraut, J. (1994) *Nat. Struct. Biol. 1*, 524−531.
6. Poulos, T. L., and Kraut, J. (1980) *J. Biol. Chem. 255*, 8199−8205.
7. Veitch, N. C. (1995) *Biochem. Soc. Trans. 23*, 232−240.
8. Critchlow, J. E., and Dunford, H. B. (1972) *J. Biol. Chem. 247*, 3703−3713.
9. Leigh, J. S., Maltempo, M. M., Ohlsson, P. I., and Paul, K. G. (1975) *FEBS Lett. 51*, 304−308.
10. Schejter, A., Lanir, A., and Epstein, N. (1976) *Arch. Biochem. Biophys. 174*, 36−44.
11. Candeias, L. P., Folkes, L. K., Porssa, M., Parrick, J., and Wardman, P. (1996) *Biochemistry 35*, 102−108.
12. Rietjens, I. M. C. M., Osman, A. M., Veeger, C., Zakharieva, O., Antony, J., Grodzicki, M., and Trautwein, A. X. (1996) *J. Biol. Inorg. Chem. 1*, 372−376.
13. Ator, M. A., and Ortiz de Montellano, P. R. (1987) *J. Biol. Chem. 262*, 1542−1551.
14. Ator, M. A., David, S. K., and Ortiz de Montellano, P. R. (1989) *J. Biol. Chem. 264*, 9250−9257.
15. Ortiz de Montellano, P. R. (1992) *Annu. Rev. Pharmacol. Toxicol. 32*, 89−107.
16. Sakurada, J., Takahashi, S., and Hosoya, T. (1986) *J. Biol. Chem. 261*, 9657−9662.
17. Thanabal, V., De Ropp, J. S., and La Mar, G. N. (1987) *J. Am. Chem. Soc. 109*, 7516−7525.
18. Veitch, N. C., and Williams, R. J. P. (1991) in *Biochemical, Molecular, and Physiological Aspects of Plant Peroxidases* (Lobarzewski, J., Greppin, H., Penel, C., and Gaspar, Th., Eds.) pp 99−109, University of Geneva, Geneva.
19. Veitch, N. C., and Williams, R. J. P. (1990) *Eur. J. Biochem. 189*, 351−362.
20. Zhao, D., Gilfoyle, D. J., Smith, A. T., and Loew, G. H. (1996) *Proteins: Struct., Funct., Genet. 26*, 204−216.
21. Veitch, N. C., Williams, R. J. P., Bone, N., Burke, J. F., and Smith, A. T. (1995) *Eur. J. Biochem. 233*, 650−658.
22. Gajhede, M., Schuller, D. J., Henriksen, A., Smith, A. T., and Poulos, T. L. (1997) *Nat. Struct. Biol. 4*, 1032−1038.
23. Veitch, N. C., Gao, Y., Smith, A. T., and White, C. G. (1997) *Biochemistry 36*, 14751−14761.
24. Schonbaum, G. R., and Lo, S. (1972) *J. Biol. Chem. 247*, 3353−3360.
25. Aviram, I. (1981) *Arch. Biochem. Biophys. 212*, 483−490.
26. Schonbaum, G. R. (1973) *J. Biol. Chem. 248*, 502−511.
27. Smulevich, G., Miller, M. A., Kraut, J., and Spiro, T. G. (1991) *Biochemistry 30*, 9546−9558.
28. Howes, B. D., Rodriguez Lopez, J. N., Smith, A. T., and Smulevich, G. (1997) *Biochemistry 36*, 1532−1543.
29. De Ropp, J. S., Mandal, P., Brauer, S. L., and La Mar, G. N. (1997) *J. Am. Chem. Soc. 119*, 4732−4739.
30. La Mar, G. N., Hernandez, G., and De Ropp, J. S. (1992) *Biochemistry 31*, 9158−9168.
31. Veitch, N. C., and Williams R. J. P. (1995) *Eur. J. Biochem. 229*, 629−640.
32. Veitch, N. C. (1993) in *Plant Peroxidases. Biochemistry and Physiology* (Welinder, K. G., Rasmussen, S. K., Penel, C., and Greppin, H., Eds.) pp 57−64, University of Geneva, Geneva.
33. Smith, A. T., Santama, N., Daceys, S., Edwards, M., Bray, R. C., Thorneley, R.-N. F., and Burke, J. F. (1990) *J. Biol. Chem. 265*, 13335−13343.
34. Matthews, B. W. (1968) *J. Mol. Biol. 33*, 491−497.
35. Otwinowski, Z. (1993) in *Proceedings of the CCP4 study weekend: Data collection and processing*, pp 56−62, SERC Daresbury Laboratory, Warrington.
36. Collaborative Computing Project, No. 4. (1994) *Acta Crystallogr. D50*, 760−763.
37. Navaza, J. (1994) *Acta Crystallogr. A50*, 157−163.
38. Schuller, D. J., Ban, N., Huystee, R. B., McPherson, A., and Poulos, T. L. (1996) *Structure 4*, 311−321.
39. Read, R. J. (1986) *Acta Crystallogr. A42*, 140−149.
40. Schuller, D. J. (1996) *Acta Crystallogr. D52*, 425−434.
41. Jones, A., Zou, J. Y., Cowan, S. W., and Kjeldgaard, M. (1991) *Acta Crystallogr. A47*, 110−119.
42. Brünger, A. T. (1992) *X-PLOR Version 3.1. A system for X-ray crystallography and NMR*, Yale University Press, New Haven.
43. Engh, R. A., and Huber, R. (1991) *Acta Crystallogr. A47*, 392−400.
44. Kleywegt, G. J., and Jones, T. A. (1996) *Acta Crystallogr. D52*, 826−828.
45. Welinder, K. G. (1976) *FEBS Lett. 72*, 19−23.
46. Edwards, S. L., and Poulos, T. L. (1990) *J. Biol. Chem. 265*, 2588−2595.
47. Veitch, N. C., Gao, Y., and Welinder, K. G. (1996) *Biochemistry 35*, 14370−14380.
48. Finzel, B. C., Poulos, T. L., and Kraut, J. (1984) *J. Biol. Chem. 259*, 13027−13036.
49. Kunishima, N., Fukuyama, K., Matsubara, H., Hatanaka, H., Shibano, Y., and Amachi, T. (1994) *J. Mol. Biol. 235*, 331−344.
50. Fukuyama, K., Kunishima, N., Amada, F., Kubota, T., and Matsubara, H. (1995) *J. Biol. Chem. 270*, 21884−21892.
51. Poulos, T. L., Edwards, S. L., Wariishi, H., and Gold, M. H. (1993) *J. Biol. Chem. 268*, 4429−4440.
52. Gilfoyle, D. J., Rodriguez Lopez, J. N., and Smith, A. T. (1996) *Eur. J. Biochem. 236*, 714−722.
53. Itakura, H., Oda, Y., and Fukuyama, K. (1997) *FEBS Lett. 412*, 107−110.
54. Berinstain, A. B., English, A. M., Hill, B. C., and Sharma, D. (1990) *J. Am. Chem. Soc. 112*, 9649−9651.
55. Piontek, K., Glumoff, T., and Winterhalter, K. (1993) *FEBS Lett. 315*, 119−124.
56. Thanabal, V., De Ropp, J. S., and La Mar, G. N. (1988) *J. Am. Chem. Soc. 110*, 3027−3035.
57. Wallace, A. C., Laskowski, R. A., and Thornton, J. M. (1995) *Protein Eng. 8*, 127−134.
58. McDonald, I. K., and Thornton, J. M. (1994) *J. Mol. Biol. 238*, 777−793.

BI980234J